

# Skyrmion-Skyrmionium Phase Separation and Laning Transitions via Spin-Orbit Torque Currents

N. P. Vizari<sup>1</sup>, J. C. Bellizotti Souza<sup>2</sup>, C. J. O. Reichhardt<sup>3</sup>, C. Reichhardt<sup>3</sup>, P. A. Venegas<sup>4</sup>, F. Béron<sup>1</sup>

<sup>1</sup> Instituto de Física “Gleb Wataghin,” Departamento de Física da Matéria Condensada, Universidade Estadual de Campinas - UNICAMP, 13083-859, Campinas, São Paulo, Brazil

<sup>2</sup> POSMAT - Programa de Pós-Graduação em Ciência e Tecnologia de Materiais, Faculdade de Ciências, Universidade Estadual Paulista - UNESP, Bauru, SP, CP 473, 17033-360, Brazil

<sup>3</sup> Theoretical Division and Center for Nonlinear Studies, Los Alamos National Laboratory, Los Alamos, New Mexico 87545, USA

<sup>4</sup> Departamento de Física, Faculdade de Ciências, Universidade Estadual Paulista - UNESP, CP 473, 17033-360 Bauru, SP, Brazil

(Dated: February 17, 2025)

Many driven binary systems can exhibit laning transitions when the two species have different mobilities, such as colloidal particles with opposite charges in electric fields. Another example is pedestrian or active matter systems, where particles moving in opposite directions form a phase-separated state that enhances the overall mobility. In this work, we use atomistic simulations to demonstrate that mixtures of skyrmions and skyrmioniums also exhibit pattern formation and laning transitions. Skyrmions move more slowly and at a finite Hall angle compared to skyrmioniums, which move faster and without a Hall effect. At low drives, the system forms a partially jammed phase where the skyrmionium is dragged by the surrounding skyrmions, resulting in a finite angle of motion for the skyrmionium. At higher drives, the system transitions into a laned state, but unlike colloidal systems, the lanes in the skyrmion-skyrmionium mixture are tilted relative to the driving direction due to the intrinsic skyrmion Hall angle. In the laned state, the skyrmionium angle of motion is reversed when it aligns with the tilted lane structure. At even higher drives, the skyrmioniums collapse into skyrmions. Below a critical skyrmion density, both textures can move independently with few collisions, but above this density, the laning state disappears entirely, and the system transitions to a skyrmion-only state. We map out the velocity and Hall responses of the different textures and identify three distinct phases: partially jammed, laned, and skyrmion-only moving crystal states. We compare our results to recent observations of tilted laning phases in pedestrian flows, where chiral symmetry breaking in the particle interactions leads to similar behavior.

## I. INTRODUCTION

Recently, there has been great interest in understanding the dynamics of interacting particles that are not all moving in the same direction. Assemblies of such particles can undergo structural transitions when subjected to external driving forces. In many cases, the particles share the same size and interaction forces; however, when the particles have different sizes or interaction strengths, order-disorder transitions may occur even in the absence of external driving<sup>1-3</sup>. Moreover, in systems where the particles are of uniform size but exhibit different dynamical behaviors, disordering transitions and other dynamical phases can emerge. For instance, in studies of oppositely driven repulsive particles, the system may form static ordered states or exhibit fluctuating disordered flow. At higher driving forces, these flows may transition into lane forming states consisting of multiple, partially phase-separated stripes of oppositely moving particles<sup>4-14</sup>. The lane arrangement minimizes collisions and enhances the efficiency of the motion<sup>14</sup>. The observation of lane formation across such diverse systems suggests that it is triggered by a universal mechanism.

In general, the lanes align with the direction of driving; however, Bacik *et al.* recently studied a pedestrian model that included a chiral symmetry-breaking effect<sup>14</sup>.

The system forms tilted lanes in which the flow is at an angle to the driving direction. This result was confirmed experimentally by asking actual pedestrians to deliberately bias their direction of motion when walking past an oppositely moving pedestrian, which adds an effective chiral term to the interaction. Although there have been numerous studies on laning behaviors in colloidal assemblies, active matter, dusty plasmas, and other systems, there are relatively few studies of the laning of particle-like magnetic textures such as skyrmions and skyrmioniums that can be supported within ferromagnets. If more than one type of magnetic texture is present simultaneously, the different textures move at different velocities for a given applied drive, providing another type of system that could exhibit laning phenomena. Unlike colloidal particles, however, many of the magnetic textures have a chiral symmetry breaking and move with a Hall angle, and might thus be expected to form tilted lanes similar to those observed by Bacik *et al.* when they added a chiral symmetry breaking term to their pedestrians. Additionally, topological transitions among different magnetic textures can occur if the driving force is sufficiently strong, so the laning dynamics of magnetic textures could be much richer than what has been observed in other systems.

Magnetic skyrmions are topologically protected

particle-like textures<sup>15–18</sup> that exhibit many similarities to particle-based systems such as type II superconducting vortices and charged colloids. Their mutually repulsive interactions cause the skyrmions to form triangular arrays<sup>15,19</sup> in order to reduce their interaction energy. Additionally, skyrmions can be set into motion by external currents<sup>20,21</sup> and can interact with defects or pinning sites, which inhibit motion below a threshold current<sup>22,23</sup>. Skyrmions are promising candidates for spintronics applications, such as memory and novel computing, due to their topological protection<sup>17,18,24</sup>, reduced size (with diameters ranging from 10 nm to  $\approx 1\mu\text{m}$ <sup>19,25,26</sup>), and their ability to be transported by spin-polarized currents<sup>20,21</sup>. Due to their topology<sup>27</sup>, under external driving skyrmions move at an angle to the applied drive known as the intrinsic skyrmion Hall angle,  $\theta_{\text{sk}}^{\text{int}}$ <sup>28–30</sup>, which has a sign that depends on the skyrmion winding number,  $Q = \pm 1$ <sup>28</sup>. The skyrmion motion thus has an effective Magnus force component that makes the skyrmion Hall angle finite and also affects how the skyrmion interacts with quenched disorder or other skyrmions. In contrast, superconducting vortices and colloidal particles typically do not have a finite Hall angle.

Skyrmionium, another particle-like magnetic texture, can be viewed as two skyrmions with opposite polarity and topological charge that have been combined into a single magnetic texture<sup>31</sup>. The concept of a skyrmionium first appeared in the literature as a “ $2\pi$  vortex”<sup>32</sup>, and in later works it was referred to as a “donut skyrmion”<sup>33</sup>, “ $2\pi$  skyrmion”<sup>34</sup>, or “target skyrmion”<sup>35</sup>. Structurally, a skyrmionium consists of a central skyrmion surrounded by an annular domain wall with an opposite topological charge, resulting in a net topological charge of  $Q = 0$ . Since the deflection of magnetic textures under an applied drive depends on the sign and magnitude of  $Q$ , skyrmioniums move without a Hall angle, making them particularly attractive for applications<sup>36</sup>. Skyrmioniums can be generated in ferromagnetic films using laser pulses<sup>37,38</sup>, and studies have shown that they can move significantly faster than skyrmions<sup>36,39–41</sup>. Methods for transporting skyrmioniums include polarized currents<sup>42</sup>, magnetic field gradients<sup>43</sup>, and spin waves<sup>44</sup>. Recent studies suggest, however, that skyrmioniums may be less dynamically stable than skyrmions. Under high driving forces, skyrmioniums can collapse into skyrmions<sup>45,46</sup>. Moreover, in materials with low Gilbert damping, skyrmioniums are prone to experiencing significant distortions, further reducing their stability<sup>39</sup>.

Although numerous studies have addressed the dynamics of skyrmions and skyrmioniums individually, the behavior of a mixed system containing both skyrmions and skyrmioniums remains unexplored. The distinct dynamical properties of these textures, such as the presence or absence of a Hall angle, differences in stability, and variations in size, could produce a wide variety of order-disorder transitions. Reichhardt and Reichhardt<sup>13</sup> studied the dynamics of mixtures of repulsive particles with

varying Magnus terms to model spinning colloidal particles in fluid flow, which could be applied to mixtures of skyrmions of different species. Under an applied external drive in the colloidal system, there is a critical driving threshold at which a Magnus-induced disordering transition can occur. The transition arises because the differing Hall angles of the two particle species cause their motions to decouple at the critical drive. At higher drive values, lane formation occurs in which the two species separate and move in distinct directions.

In this work, we perform atomistic simulations of skyrmions and skyrmioniums coexisting within the same ferromagnetic thin film. For systems with a single skyrmionium among multiple skyrmions, we observe distinct behaviors depending on the skyrmion density. At intermediate skyrmion densities, there is an interplay between the motion of the skyrmions and the skyrmionium. In this regime, the skyrmionium exhibits a positive nonzero angle of motion relative to the driving direction while the skyrmions continue to move in a direction close to their intrinsic skyrmion Hall angle. At high skyrmion densities, the skyrmionium is dragged along with the skyrmions, moving at an angle closer to the intrinsic skyrmion Hall angle. Interestingly, for intermediate skyrmion densities, the difference in velocity between the skyrmions and the skyrmionium permits the skyrmionium to open a dynamic lane through the skyrmions. In this state, the skyrmionium can travel with a high velocity, and there is a clear phase separation between the skyrmion and skyrmionium species. When additional skyrmioniums are introduced into the system, they can follow and reinforce skyrmionium lanes that have been established through the skyrmions, thereby enhancing their collective motion. Beyond skyrmion and skyrmionium mixtures, other possible mixed magnetic textures include skyrmion–antiskyrmion combinations<sup>47,48</sup>, skyrmions and skyrmion bundles<sup>49</sup>, skyrmions and chiral bobbles<sup>50</sup>, and coexisting tubular and partial skyrmion phases<sup>51</sup>. Similarly, in liquid crystal systems, different textures with varying mobilities can coexist<sup>52–54</sup>. These findings suggest that magnetic textures are a fruitful class of systems in which to study lane formation effects.

## II. SIMULATION

We simulate the collective behavior of  $N_{\text{skium}}$  skyrmioniums among  $N_{\text{sk}}$  skyrmions in an ultrathin ferromagnetic material at  $T = 0$  K that can host Néel skyrmions. The film has dimensions of  $L \times L$ , where  $L = 136$  nm, and has periodic boundary conditions along the  $x$  and  $y$  directions. A magnetic field is applied perpendicular to the film surface. The skyrmionium density is  $n_{\text{skium}} = N_{\text{skium}}/L^2$  and the skyrmion density is  $n_{\text{sk}} = N_{\text{sk}}/L^2$ . We perform the simulations for several ratios of  $N_{\text{skium}}/N_{\text{sk}}$  in order to characterize the skyrmionium-skyrmion behavior under the application of a spin-orbit-torque (SOT) current. In Fig. 1 we illustrate

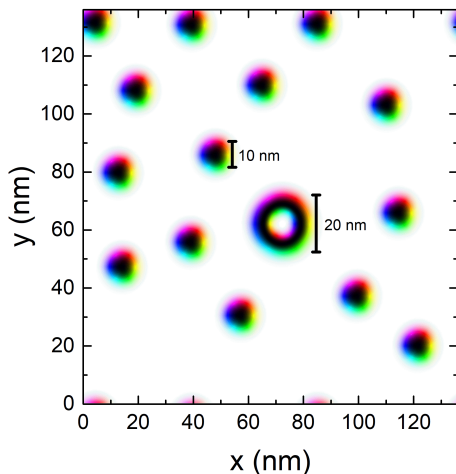


FIG. 1. Illustration of a representative sample containing  $N_{\text{sk}} = 14$  skyrmions and  $N_{\text{skium}} = 1$  skyrmionium after the stabilization process at zero current,  $j = 0$  A/m<sup>2</sup>. The magnetic textures are visualized by projecting the magnetic moments onto the  $xy$  plane. The skyrmions and skyrmionium were initially placed at random positions, and their average diameters are approximately 10 and 20 nm, respectively.

a representative sample containing  $N_{\text{skium}} = 1$  skyrmionium and  $N_{\text{sk}} = 14$  skyrmions.

The skyrmion and skyrmionium behavior is described using the atomistic model<sup>55</sup>, which captures the dynamics of individual atomic magnetic moments. This method allow us to investigate the spin textures in detail. The Hamiltonian governing the atomistic dynamics is given by<sup>29,55,56</sup>,

$$\mathcal{H} = - \sum_{i,j \in n.n.} J_{ij} \mathbf{m}_i \cdot \mathbf{m}_j - \sum_{i,j \in n.n.} \mathbf{D}_{ij} \cdot (\mathbf{m}_i \times \mathbf{m}_j) \quad (1)$$

$$- \sum_i \mu \mathbf{H} \cdot \mathbf{m}_i - \sum_i K (\mathbf{m}_i \cdot \hat{\mathbf{z}})^2 .$$

The underlying lattice is a square arrangement of atomic spins with lattice constant  $a = 0.5$  nm. The first term on the right side of Eq. (1) is the exchange interaction between nearest neighbor magnetic moments  $i$  and  $j$  with an exchange constant of  $J_{ij} = J$ . The second term is the interfacial Dzyaloshinskii–Moriya (DM) interaction, where  $\mathbf{D}_{ij} = D \hat{\mathbf{z}} \times \hat{\mathbf{r}}_{ij}$  is the DM vector between magnetic moments  $i$  and  $j$ ,  $D$  is the DM constant, and  $\hat{\mathbf{r}}_{ij}$  is the unit distance vector between atomic sites  $i$  and  $j$ . The DM term is what stabilizes the Néel skyrmions and skyrmioniums. The third term is the Zeeman interaction with an applied external magnetic field  $\mathbf{H}$ , and the fourth term is the sample anisotropy with strength  $K$ . Here  $\mu = \hbar\gamma$  is the magnitude of the magnetic moment and  $\gamma = 1.76 \times 10^{11}$  T<sup>-1</sup> s<sup>-1</sup> is the electron gyromagnetic ratio. Since we are considering ultrathin films, long-range dipolar interactions can be neglected as they are expected to be very small<sup>57</sup>.

The time evolution for the individual atomic magnetic

moments is obtained from the Landau-Lifshitz-Gilbert equation augmented with the SOT current<sup>58,59</sup>:

$$\frac{\partial \mathbf{m}_i}{\partial t} = -\gamma \mathbf{m}_i \times \mathbf{H}_i^{\text{eff}} + \alpha \mathbf{m}_i \times \frac{\partial \mathbf{m}_i}{\partial t} + \frac{j \hbar \gamma P a^2}{2e\mu} \mathbf{m} \times (\hat{\mathbf{j}} \times \hat{\mathbf{z}}) \times \mathbf{m} . \quad (2)$$

Here  $\mathbf{H}_i^{\text{eff}} = -\frac{1}{\hbar\gamma} \frac{\partial \mathcal{H}}{\partial \mathbf{m}_i}$  is the effective magnetic field, including all interactions from the Hamiltonian,  $\alpha$  is the phenomenological damping introduced by Gilbert, and the last term is the torque induced by the SOT current, where  $j$  is the current density,  $P = 1$  is the spin polarization,  $e$  is the electron charge, and  $a$  is the lattice parameter. We fix  $\mu \mathbf{H} = 0.5(D^2/J)\hat{\mathbf{z}}$  and  $\alpha = 0.4$ . In all cases, the external current  $\mathbf{j}$  is applied along  $-\hat{\mathbf{x}}$ , which results in a driving force along  $-\hat{\mathbf{x}}$  in both magnetic textures; however, since skyrmions have a topological charge of  $Q = \pm 1$ , they exhibit a finite skyrmion Hall angle<sup>28,41,46</sup>. The material parameters are  $J = 1$  meV,  $D = 0.2J$ , and  $K = 0.01J$ . These material parameters stabilize Néel skyrmions similar to those found for Pt/Co/MgO thin-films<sup>60</sup>.

For each simulation, we place a selected number of skyrmions and skyrmioniums randomly throughout the sample and perform a simulated annealing process using a stochastic gradient descent (SGD) method<sup>61,62</sup>. The system settles into a ground state that we use as input for the dynamics. The numerical integration of Eq. 2 is performed using a fourth order Runge-Kutta method. For each value of  $j$ , we calculate the time average velocity components,  $\langle v_x \rangle_{\text{sk,skium}}$  and  $\langle v_y \rangle_{\text{sk,skium}}$ , for the skyrmions and skyrmionium(s), respectively, over 200 ns to ensure a steady state measurement.

### III. SINGLE SKYRMIONIUM AMONG MULTIPLE SKYRMIONS

We first consider a single skyrmionium stabilized among 14 skyrmions. Figure 1 shows the static configuration of this system under zero external drive,  $j = 0$  A/m<sup>2</sup>. In Fig. 2 we plot the average skyrmionium and skyrmion velocity components  $\langle V_x \rangle_{\text{sk,skium}}$  and  $\langle V_y \rangle_{\text{sk,skium}}$  along with the skyrmionium and skyrmion angle of motion  $\theta_{\text{sk,skium}}$  with respect to the drive as a function of the external current,  $j$ . We find that the skyrmion velocity components  $\langle V_x \rangle_{\text{sk}}$  and  $\langle V_y \rangle_{\text{sk}}$  increase monotonically with drive. In contrast, for the skyrmionium,  $\langle V_y \rangle_{\text{skium}}$  exhibits a sudden reversal in sign at  $j = 1.25 \times 10^9$  A/m<sup>2</sup>, indicating that the skyrmionium has changed its direction of motion. At this same current,  $\langle V_x \rangle_{\text{skium}}$  increases in magnitude. Figure 2(b) shows that the direction of motion of the skyrmions barely changes with drive but remains very close to  $\theta_{\text{sk}} \approx 67^\circ$  for all values of  $j$ . The skyrmionium direction of motion, on the other hand, exhibits a complete reversal from  $\theta_{\text{skium}} \approx 9^\circ$  to  $\theta_{\text{skium}} \approx -9^\circ$ . The velocity and direction of motion changes exhibited by the skyrmionium are signatures of a dynamic transition. For  $j \leq 1.00 \times 10^9$  A/m<sup>2</sup> the system

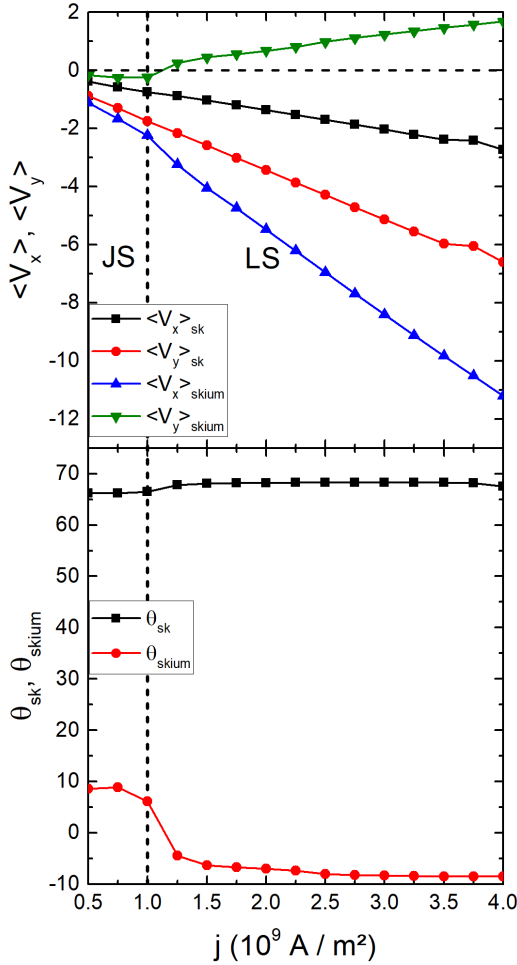


FIG. 2. (a) The velocity components  $\langle V_x \rangle_{\text{skium,sk}}$  and  $\langle V_y \rangle_{\text{skium,sk}}$  and (b) the corresponding angle of motion  $\theta_{\text{skium,sk}}$  with respect to the drive vs the external drive  $j$  for the sample illustrated in Fig. 1 with  $N_{\text{skium}} = 1$  skyrmionium among  $N_{\text{sk}} = 14$  skyrmions. The dashed vertical line separates the jammed state (JS) from the laning state (LS). The dashed horizontal line in (a) highlights the transition from negative to positive velocity values.

is in a partially jammed state (JS) where the skyrmionium is dragged along by the skyrmions, giving it a finite and positive angle of motion. When the skyrmionium collides with the skyrmions, it deviates from its natural trajectory, which in the absence of other textures or defects would be along  $\theta_{\text{skium}} = 0^\circ$ <sup>36</sup>. The jamming effect is relatively weak due to the moderate skyrmion density. For  $j > 1.00 \times 10^9 \text{ A/m}^2$ , the system transitions to a laning state (LS), where the skyrmionium is able to open a path through the skyrmions and flow at higher velocity while experiencing few to no collisions with the skyrmions. In Fig. 3(a) we illustrate the skyrmionium and skyrmion trajectories for the partially jammed state at  $j = 0.75 \times 10^9 \text{ A/m}^2$  and in Fig. 3(b) we show the same for the laning state at  $j = 1.50 \times 10^9 \text{ A/m}^2$ . In the partially jammed state, the skyrmionium moves along the

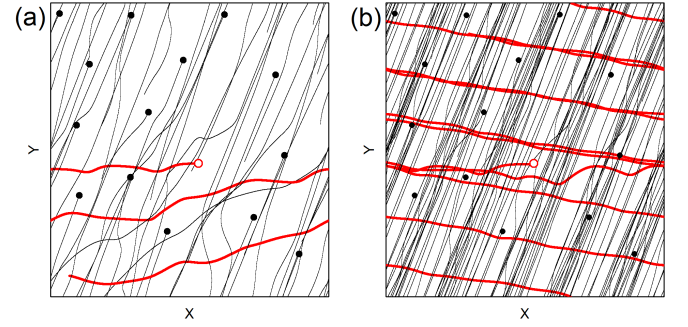


FIG. 3. Illustration of the skyrmion (black) and skyrmionium (red) trajectories for the sample from Fig. 1 with  $N_{\text{skium}} = 1$  and  $N_{\text{sk}} = 14$  over a time interval of  $\Delta t = 200 \text{ ns}$ . (a) The JS at  $j = 0.75 \times 10^9 \text{ A/m}^2$ . (b) The LS at  $j = 1.50 \times 10^9 \text{ A/m}^2$ . The large black dots indicate the initial positions of the skyrmions, and the open red circle is the initial position of the skyrmionium.

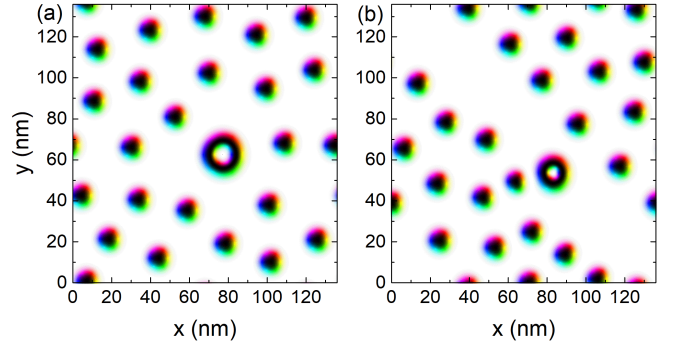


FIG. 4. Snapshots of a system with  $N_{\text{sk}} = 25$  and  $N_{\text{skium}} = 1$ . (a) The ground state at  $j = 0 \text{ A/m}^2$ . (b) The laning state at  $j = 2.25 \times 10^9 \text{ A/m}^2$ . The magnetic textures are visualized by projecting the magnetic moments onto the  $xy$  plane.

$-x$  and  $-y$  directions, and its motion is tortuous due to the collisions with the skyrmions that are traveling along  $-x$  and  $-y$  at a larger angle of motion. The skyrmion trajectories are also tortuous due to collisions with the skyrmionium and other skyrmions. In the laning state, the skyrmionium moves along the  $-x$  and  $+y$  direction, as also shown in Fig. 2. The trajectories of both the skyrmionium and skyrmions are less tortuous since the opening of a lane for skyrmionium motion minimizes the number of skyrmionium-skyrmion collisions that occur.

In Fig. 4(a) we show the  $j = 0$  ground state of a system with  $N_{\text{sk}} = 25$  and  $N_{\text{skium}} = 1$ . Although the number of skyrmions in the sample is now larger, the skyrmionium and skyrmion sizes remain roughly the same as in the  $N_{\text{sk}} = 14$  and  $N_{\text{skium}} = 1$  sample shown in Fig. 1. Note that the empty space surrounding the skyrmionium is relatively larger than that separating adjacent skyrmions. This is the result of the larger repulsive interaction exhibited by skyrmionium<sup>46</sup>.

In Fig. 5 we plot  $\langle V_x \rangle_{\text{sk,skium}}$ ,  $\langle V_y \rangle_{\text{sk,skium}}$  and  $\theta_{\text{sk,skium}}$  versus  $j$  for the  $N_{\text{sk}} = 25$  and  $N_{\text{skium}} = 1$  system. Fig-

ure 5(a) shows that the skyrmion velocity components  $\langle V_x \rangle_{\text{sk}}$  and  $\langle V_y \rangle_{\text{sk}}$  increase linearly in magnitude with increasing drive, very similar to the behavior that appears in Fig. 2. Here the skyrmions dominate the behavior of the sample, and their dynamics remain largely unaffected by the presence of the skyrmionium. Similarly, in Fig. 5(b), the skyrmion angle of motion  $\theta_{\text{sk}} \approx 67^\circ$  for all values of  $j$ . As more skyrmions are added and the skyrmion density increases, the influence of the skyrmionium on the skyrmion dynamics diminishes even further. We find that for the skyrmionium,  $\langle V_x \rangle_{\text{skium}}$  and  $\langle V_y \rangle_{\text{skium}}$  are separable into two regimes: a partially jammed state for  $j < 1.25 \times 10^9 \text{ A/m}^2$ , and a laning state for  $j \geq 1.25 \times 10^9 \text{ A/m}^2$ . As was the case in Fig. 2, in the partially jammed state the skyrmionium is dragged along by the skyrmions and moves along a nonzero angle to the driving direction. Due to the higher skyrmion density in the  $N_{\text{sk}} = 25$  sample compared to the  $N_{\text{sk}} = 14$  sample,  $\theta_{\text{skium}} \approx 18^\circ$  in the partially jammed state of Fig. 5(b) is larger than the value  $\theta_{\text{skium}} \approx 9^\circ$  found in Fig. 2(b). In addition, in the laning state of Fig. 5(a), due to the higher skyrmion density  $\langle V_y \rangle_{\text{skium}}$  approaches zero but never becomes positive. As the external drive  $j$  increases in magnitude, the skyrmions and skyrmionium both travel at higher velocities, causing stronger deformations and shrinkages to occur during each collision. The consequences are illustrated in Fig. 4(b) at  $j = 2.25 \times 10^9 \text{ A/m}^2$ , where the laning state is well-established, but where collisions with skyrmions have caused the skyrmionium to shrink from its ground state size of  $d \approx 20 \text{ nm}$  to only  $d \approx 15 \text{ nm}$ . The skyrmionium moves at a much higher velocity than the skyrmions, which facilitates the phase separation, but also increases the pressure on the skyrmionium due to the nearly constant contact with the skyrmions at the edge of the lane. For  $j > 2.50 \times 10^9 \text{ A/m}^2$ , the pressure on the skyrmionium becomes so large that the internal skyrmion of the skyrmionium annihilates, transforming the skyrmionium into an ordinary skyrmion. This is why no skyrmionium velocity or angle of motion measurements appear in Fig. 5 above  $j > 2.50 \times 10^9 \text{ A/m}^2$ . The resulting state, where only coherently moving skyrmions are present in the system, is called the moving skyrmion lattice (MSk).

For the  $N_{\text{skium}} = 1$  and  $N_{\text{sk}} = 25$  sample, the skyrmion trajectories are illustrated in the JS at  $j = 0.75 \times 10^9 \text{ A/m}^2$  in Fig. 6(a) and in the LS for  $j = 2.25 \times 10^9 \text{ A/m}^2$  in Fig. 6(b). The behavior is similar to that found in Fig. 3. In the JS shown in Fig. 6(a), the trajectories are more tortuous due to the skyrmion-skyrmion collisions and the dragging of the skyrmionium by the skyrmions. In the LS shown in Fig. 6(b), the trajectories are straighter and the skyrmionium moves with an average angle of  $\theta_{\text{skium}} \approx 0^\circ$ .

We performed a series of simulations for varied currents  $j$  and skyrmion densities  $n_{\text{sk}}$  in order to construct the dynamic phase diagram shown in Fig. 7. The LS appears in the range  $0.00027 < n_{\text{sk}} < 0.00189$ . If the

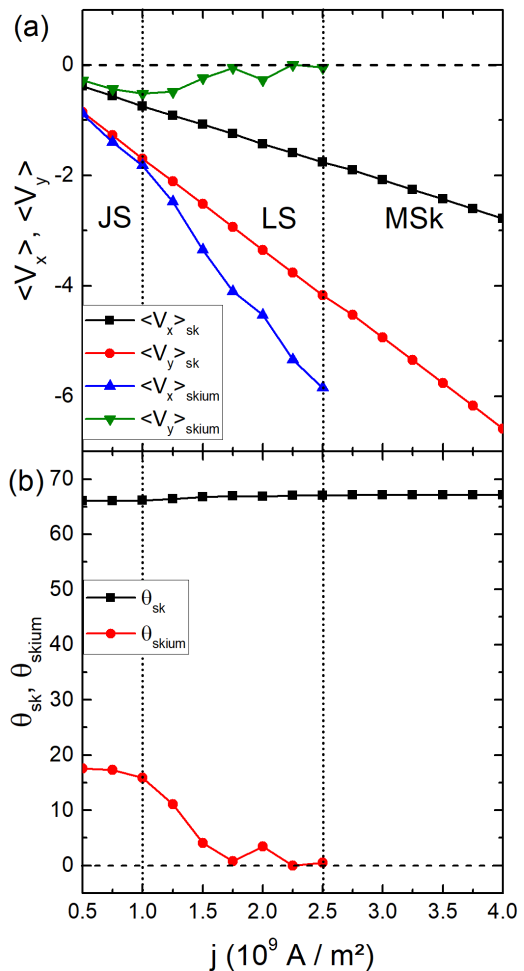


FIG. 5. (a) The velocity components  $\langle V_x \rangle_{\text{skium,sk}}$  and  $\langle V_y \rangle_{\text{skium,sk}}$  and (b) the corresponding angle of motion  $\theta_{\text{skium,sk}}$  with respect to the external drive  $j$  plotted vs  $j$  for the  $N_{\text{skium}} = 1$  and  $N_{\text{sk}} = 25$  sample from Fig. 4(a). The dashed vertical lines separate the partially jammed state (JS), laning state (LS), and moving skyrmion lattice (MSk) state. The dashed horizontal line in (a) highlights the transition from negative to positive velocity values.

skyrmionium is placed in a very sparse system with a low density of skyrmions, both textures move independently and undergo very few collisions, a regime that we label as independent dynamics (ID). This phase is stable for very low skyrmion densities,  $n_{\text{sk}} \leq 0.00038$ . Lane formation is still possible in the ID state because the skyrmionium can influence the motion of the skyrmions through collisions and generate a phase separation between the textures. The direction of motion of the skyrmionium is, however, barely changed in the ID regime, so the system is not behaving as a partially jammed solid. When the skyrmion density is large,  $n_{\text{sk}} \geq 0.00189$ , the skyrmionium is no longer able to separate itself from the skyrmions through a laning process and is strongly dragged by the skyrmion lattice in the JS until skyrmionium annihilation occurs for higher drives. Phase separation can

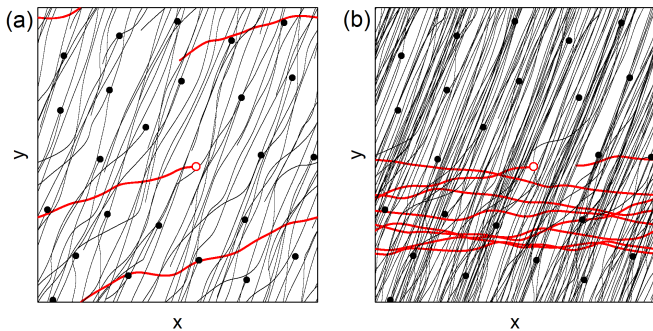


FIG. 6. Illustration of the skyrmion (black) and skyrmionium (red) trajectories for the sample from Fig. 4 with  $N_{\text{skium}} = 1$  and  $N_{\text{sk}} = 25$  over a time interval of  $\Delta t = 200$  ns. (a) The JS at  $j = 0.75 \times 10^9$  A/m<sup>2</sup>. (b) The LS at  $j = 2.25 \times 10^9$  A/m<sup>2</sup>. The large black dots indicate the initial positions of the skyrmions, and the open red circle is the initial position of the skyrmionium.

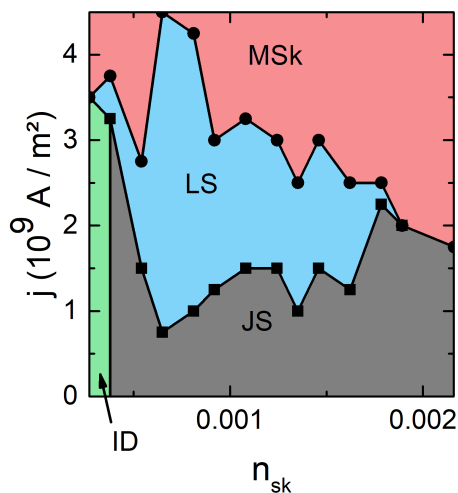


FIG. 7. Dynamic phase diagram as a function of  $j$  vs skyrmion density  $n_{\text{sk}}$  for samples containing  $N_{\text{skium}} = 1$  skyrmionium. Green: independent dynamics (ID); gray: partially jammed state (JS); light blue: laning state (LS); red: moving skyrmion lattice (MSk).

only occur when the driving is sufficiently large. For  $j < 0.75 \times 10^9$  A/m<sup>2</sup>, the LS never appears since the skyrmionium does not have sufficient energy to separate from the skyrmion phase at any skyrmion density. At  $n_{\text{sk}} = 0.00065$ , lane formation is optimized and the LS extends from  $j = 0.75 \times 10^9$  A/m<sup>2</sup> all the way up to  $j = 4.50 \times 10^9$  A/m<sup>2</sup>. This is very similar to the lane formation discussed in detail in Figs. 2 and 3 for  $n_{\text{sk}} = 0.00081$ . If the external current becomes too strong, however, the internal skyrmion of the skyrmionium is annihilated due to collisions with skyrmions, causing the skyrmionium to transform into a skyrmion and resulting in the appearance of a moving skyrmion lattice phase (MSk).

#### IV. MULTIPLE SKYRMIONIUMS AMONG MULTIPLE SKYRMIONS

We now move from the single skyrmionium regime to multiple skyrmioniums. In Fig. 8 we plot  $\langle V_x \rangle_{\text{sk,skium}}$ ,  $\langle V_y \rangle_{\text{sk,skium}}$ , and  $\theta_{\text{sk,skium}}$  versus  $j$  for a system with  $N_{\text{skium}} = 3$  and  $N_{\text{sk}} = 10$ . The skyrmion velocity components  $\langle V_x \rangle_{\text{sk}}$  and  $\langle V_y \rangle_{\text{sk}}$  in Fig. 8(a) are no longer linear because the dynamics of the skyrmions are now strongly impacted by the presence of the skyrmioniums. The skyrmion angle of motion is also affected, as illustrated in the plot of  $\theta_{\text{sk}}$  versus  $j$  in Fig. 8(b), where the skyrmion angle oscillates around  $\theta_{\text{sk}} \approx 69^\circ$ . The laning state (LS) appears at low drives,  $j > 0.75 \times 10^9$  A/m<sup>2</sup>. As more skyrmioniums are added to the sample, it becomes easier for them to establish stable phase separated lanes passing through the skyrmions since each skyrmionium can reinforce the lane opened by the skyrmionium traveling ahead of it. We show snapshots from the system in Fig. 8 at zero external drive in Fig. 9(a), in the JS where the skyrmions and skyrmioniums are mixed together at  $j = 0.75 \times 10^9$  A/m<sup>2</sup> in Fig. 9(b), in the LS at  $j = 2.25 \times 10^9$  A/m<sup>2</sup> in Fig. 9(c), and in the MSk state at  $j = 3.75 \times 10^9$  A/m<sup>2</sup> in Fig. 9(d), where all of the skyrmioniums have been transformed into skyrmions and the entire system flows along the intrinsic Hall angle of  $\theta_{\text{sk}}^{\text{int}} = 67^\circ$ .

In Fig. 10 we plot  $\langle V_x \rangle_{\text{sk,skium}}$ ,  $\langle V_y \rangle_{\text{sk,skium}}$ , and  $\theta_{\text{sk,skium}}$  versus  $j$  for a system with  $N_{\text{skium}} = 2$  and  $N_{\text{sk}} = 26$ . The stability region of the JS is increased relative to what we have shown up to this point, and extends over  $j < 2.5 \times 10^9$  A/m<sup>2</sup>. The LS is only stable over a narrow range of currents,  $2.5 \times 10^9$  A/m<sup>2</sup>  $< j \leq 2.75 \times 10^9$  A/m<sup>2</sup>. For  $j > 2.75 \times 10^9$  A/m<sup>2</sup>, all of the skyrmioniums annihilate and the system enters the MSk phase. Two skyrmioniums are present in the sample throughout the entire JS, as illustrated in Fig. 11(a) at  $j = 1.50 \times 10^9$  A/m<sup>2</sup>. That is, both of the skyrmioniums have become jammed among the skyrmions and are not able to create a path for phase separation and lane formation. When  $j > 2.50 \times 10^9$  A/m<sup>2</sup>, however, one of the skyrmioniums transforms into a skyrmion, reducing the total effective density of the sample slightly and enabling the skyrmions to compress enough that the remaining skyrmionium can establish laning flow, resulting in the formation of the LS shown in Fig. 10. A snapshot of the LS at  $j = 2.75 \times 10^9$  A/m<sup>2</sup> appears in Fig. 11(b), where the sample contains 27 skyrmions and only one skyrmionium. Upon further increasing the drive, the remaining skyrmionium annihilates and only skyrmions remain in the sample, very similar to the snapshot shown in Fig. 9(d).

Combining multiple skyrmioniums with multiple skyrmions produces a much more complex behavior than when there is only a single skyrmionium present. When the skyrmion density is not too high, multiple skyrmioniums can cooperate with each other to form lanes and

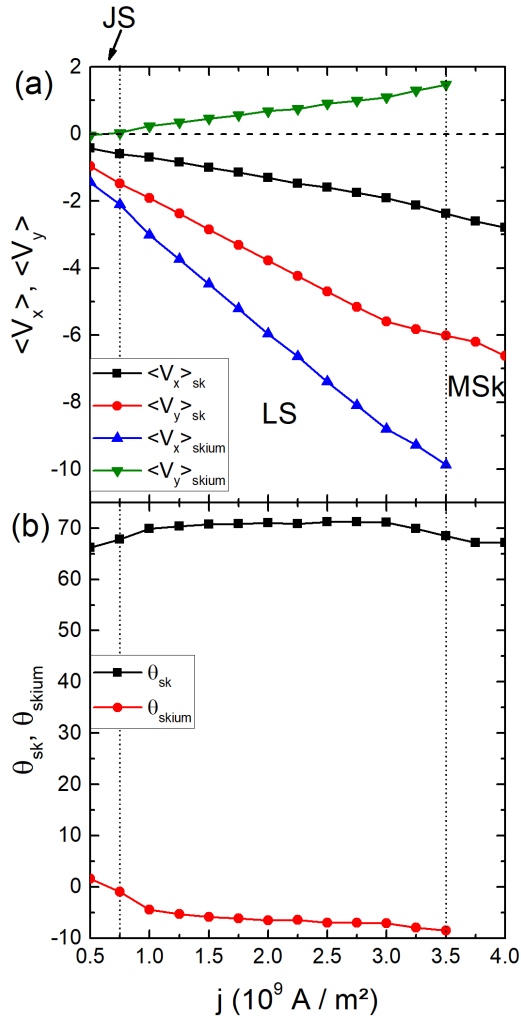


FIG. 8. (a) The velocity components  $\langle V_x \rangle_{\text{skium,sk}}$  and  $\langle V_y \rangle_{\text{skium,sk}}$  and (b) the corresponding angle of motion  $\theta_{\text{skium,sk}}$  with respect to the external drive  $j$  plotted vs  $j$  for the  $N_{\text{skium}} = 3$  and  $N_{\text{sk}} = 10$  sample illustrated in Fig. 9(a). The dashed vertical lines separate the jammed state (JS), laning state (LS) and moving skyrmion lattice (MSk). The dashed horizontal line in (a) highlights the transition from negative to positive velocity values.

expand the window in which the LS is stable. Due to the differences in sizes and dynamics between the skyrmions and the skyrmioniums, when the skyrmion density is high, there is not enough free space available for multiple skyrmioniums to create a path, and the JS is stabilized over a wide range of  $j$  values. The formation of lanes becomes possible only when a portion of the skyrmioniums annihilate and create more free space for lane formation.

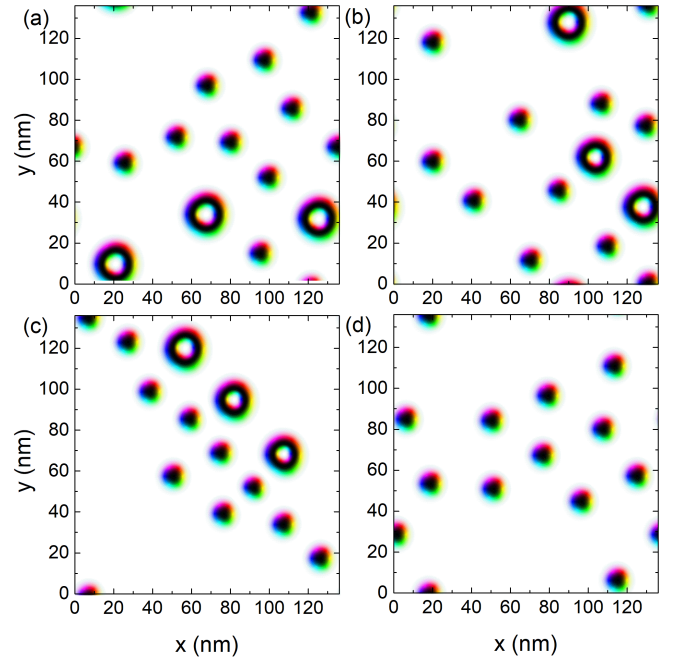


FIG. 9. Snapshots of a system with  $N_{\text{sk}} = 10$  and  $N_{\text{skium}} = 3$ . (a) The ground state at  $j = 0 \text{ A/m}^2$ . (b) The partially jammed state (JS) at  $j = 0.75 \times 10^9 \text{ A/m}^2$ . (c) The laning state (LS) at  $j = 2.25 \times 10^9 \text{ A/m}^2$ . (d) The moving skyrmion lattice state (MSk) at  $j = 3.75 \times 10^9 \text{ A/m}^2$ . The magnetic textures are visualized by projecting the magnetic moments onto the  $xy$  plane.

## V. MORE SKYRMIONIUMS THAN SKYRMIONS

We have shown that when the number of skyrmions is larger than the number of skyrmioniums, phase separation of the two species can occur in the form of the emergence of a laning state, and that this process depends strongly on the skyrmion density. In this section we investigate what happens when the ferromagnetic film contains more skyrmioniums than skyrmions by preparing a sample with  $N_{\text{sk}} = 8$  and  $N_{\text{skium}} = 12$ , as illustrated in Fig. 12(a).

In Fig. 13, the plot of  $N_{\text{sk}}$  and  $N_{\text{skium}}$  versus  $j$  shows that skyrmioniums are progressively being collapsed into skyrmions as the driving current  $j$  increases. At low drives of  $j \leq 1.00 \times 10^9 \text{ A/m}^2$ , there is not enough compression of the skyrmioniums by the current and collisions with other textures to collapse the skyrmioniums into skyrmions. In this low drive regime, a JS appears in which phase separation between skyrmions and skyrmioniums does not occur. Note that the number of skyrmions and skyrmioniums present may change depending on the precise value of the current, but in general about half of the textures are skyrmioniums and the other half are skyrmions. For intermediate drives,  $1.00 \times 10^9 \text{ A/m}^2 < j \leq 3.00 \times 10^9 \text{ A/m}^2$ , a LS forms. At these values of  $j$ , a portion of the skyrmioniums col-

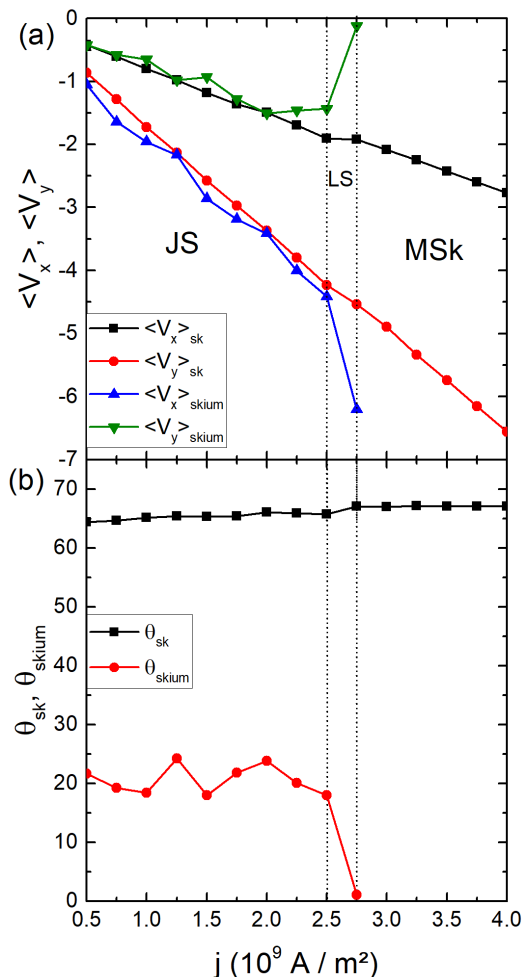


FIG. 10. (a) The velocity components  $\langle V_x \rangle_{\text{skium,sk}}$  and  $\langle V_y \rangle_{\text{skium,sk}}$  and (b) the corresponding angle of motion  $\theta_{\text{skium,sk}}$  with respect to the external drive  $j$  plotted vs  $j$  for the  $N_{\text{skium}} = 2$  and  $N_{\text{sk}} = 26$  sample illustrated in Fig. 11(a). The dashed vertical lines separate the partially jammed state (JS), laning state (LS), and moving skyrmion lattice (MSk) state.

lapse into skyrmions, which provides enough free space for lane formation and phase separation to occur. As the drive increases, the number of skyrmioniums continues to fall and the number of skyrmions continues to increase. It is important to note that the ground state in Fig. 12(a) is densely packed since the repulsive interactions between skyrmionium pairs is larger than that of skyrmion pairs<sup>46</sup>, making a skyrmionium array effectively more dense than a skyrmion array containing the same number of magnetic textures. Thus, when skyrmioniums are replaced by skyrmions at the higher drives, this effectively creates more space for lane formation. For high drives of  $j > 3.00 \times 10^9 \text{ A/m}^2$ , the current is strong enough to annihilate all of the skyrmioniums present in the sample, leading to the formation of the MSk phase.

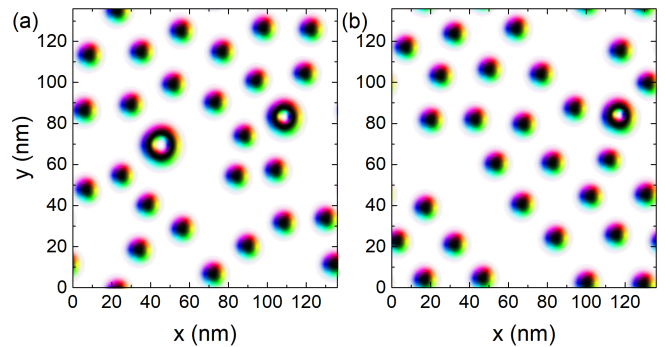


FIG. 11. Snapshots of a system with an initial state of  $N_{\text{sk}} = 26$  and  $N_{\text{skium}} = 2$ . (a) The partially jammed state (JS) at  $j = 1.50 \times 10^9 \text{ A/m}^2$ , where the number of skyrmions and skyrmioniums is unchanged. (b) The laning state (LS) at  $j = 2.75 \times 10^9 \text{ A/m}^2$ , where there are now 27 skyrmions and 1 skyrmionium. The magnetic textures are visualized by projecting the magnetic moments onto the  $xy$  plane.

## VI. DISCUSSION

Our atomistic simulations allow us to investigate the conditions under which skyrmioniums and skyrmions can be stabilized in ferromagnetic thin films with a perpendicular applied magnetic field at zero temperature. We transport the magnetic textures via spin-orbit torque (SOT); however, it should be possible to transport skyrmions and skyrmioniums via spin-transfer torque (STT) with non-adiabatic terms. A STT current without a non-adiabatic term can only transport the skyrmions but would not transport the skyrmioniums. In this case, the moving skyrmions would drag the passive skyrmioniums through the sample, which would probably cause the skyrmioniums to collapse into skyrmions beginning at relatively low currents. A STT current with non-adiabatic terms would move both textures at the same velocity but along different directions<sup>41</sup>. This would be an interesting topic to address in future work, since lane formation might still occur, but the stability of the lanes might be affected. Other alternative methods for transporting the textures could also be investigated, such as spin waves, magnetic fields, or temperature gradients<sup>44,63–65</sup>. We have not considered thermal effects in our simulations; however, we expect that mild temperature effects could facilitate the penetration of the skyrmionium into the skyrmion lattice and enhance the phase separation. Still, since the skyrmioniums are less stable than the skyrmions, higher temperatures could lead to the premature annihilation of the inner skyrmion of the skyrmionium<sup>66</sup>.

## VII. SUMMARY

We have investigated the dynamical phase separation and laning transitions of driven skyrmion–skyrmionium

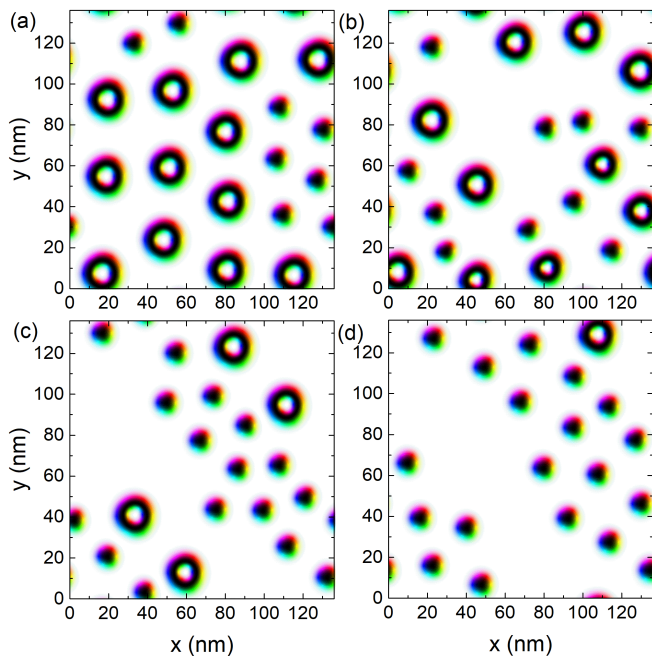


FIG. 12. Snapshots of a system with an initial state of  $N_{\text{sk}} = 8$  and  $N_{\text{skium}} = 12$ . (a) The ground state at  $j = 0 \text{ A/m}^2$ . (b) The jammed state (JS) at  $j = 1.00 \times 10^9 \text{ A/m}^2$ , where half of the textures are skyrmions and the other half are skyrmioniums. (c) The laning state (LS) at  $j = 2.00 \times 10^9 \text{ A/m}^2$ , where there are 4 skyrmioniums and 16 skyrmions. (d) The laning state (LS) at  $j = 3.00 \times 10^9 \text{ A/m}^2$ , where there is a single skyrmionium and 19 skyrmions. The magnetic textures are visualized by projecting the magnetic moments onto the  $xy$  plane.

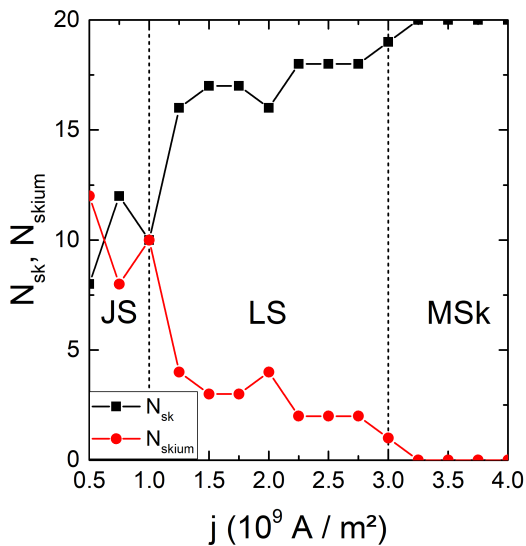


FIG. 13. The number of skyrmions,  $N_{\text{sk}}$ , and skyrmioniums,  $N_{\text{skium}}$ , present in the sample as a function of the external driving current  $j$  for the system from Fig. 12 that was initialized with  $N_{\text{sk}} = 8$  and  $N_{\text{skium}} = 12$ . The vertical dashed lines separate the jammed state (JS), laning state (LS), and moving skyrmion lattice (MSk).

mixtures using atomistic simulations. Skyrmions move at

a finite Hall angle, while skyrmioniums exhibit no Hall effect and move at twice the speed of the skyrmions. For a single skyrmionium in a bath of skyrmions, we observe a low-drive, partially jammed phase in which the skyrmions induce a finite angle of motion for the skyrmionium motion due to an effective drag effect. At higher drives, the system transitions into a laned state, with the lanes tilted opposite to the Hall angle of the skyrmions. This results in a reversal of the skyrmionium angle of motion, as the motion of the skyrmionium is partially guided by the tilted lane structure. When the skyrmion density is increased, we find a high drive state in which the skyrmionium collapses into a skyrmion. For mixtures containing multiple skyrmioniums, we observe a partially jammed state in which the skyrmioniums acquire a finite angle of motion along the direction of the skyrmion motion, as well as a laned state where a finite skyrmionium angle of motion persists. At sufficiently high drives, the skyrmioniums once again collapse into skyrmions. For certain ratios of skyrmioniums to skyrmions, we find more strongly jammed states in which the skyrmions and skyrmioniums move together as a rigid cluster with suppressed laning. Above a critical skyrmion density, the system transitions directly into a fully jammed skyrmion state that contains no skyrmioniums. Unlike what is observed in colloidal systems, the lanes in our system are tilted relative to the driving direction, similar to the tilted lanes recently observed for pedestrian crowds moving in opposite directions with chiral rules of motion. In the skyrmion/skyrmionium system, the chirality arises from the finite skyrmion Hall angle. We map out a dynamic phase diagram as a function of current and skyrmion density. Although our results focus on skyrmion-skyrmionium mixtures, we expect similar laning transitions to occur for mixtures of other magnetic textures that have different Hall angles or mobilities. Our findings indicate that mixtures of magnetic textures with distinct topologies represent a promising and fruitful class of systems for exploring laning transitions and collective dynamics.

## ACKNOWLEDGMENTS

This work was supported by the US Department of Energy through the Los Alamos National Laboratory. Los Alamos National Laboratory is operated by Triad National Security, LLC, for the National Nuclear Security Administration of the U. S. Department of Energy (Contract No. 892333218NCA000001). N.P.V. acknowledges funding from Fundação de Amparo à Pesquisa do Estado de São Paulo - FAPESP (Grant 2024/13248-5). J.C.B.S. acknowledges funding from Fundação de Amparo à Pesquisa do Estado de São Paulo - FAPESP (Grant 2021/04941-0). We would like to thank FAPESP for providing the computational resources used in this work (Grant: 2024/02941-1).

- <sup>1</sup> M. R. Sadr-Lahijany, P. Ray, and H. E. Stanley, “Dispersivity-driven melting transition in two-dimensional solids,” *Phys. Rev. Lett.* **79**, 3206–3209 (1997).
- <sup>2</sup> T. Hamanaka and A. Onuki, “Transitions among crystal, glass, and liquid in a binary mixture with changing particle-size ratio and temperature,” *Phys. Rev. E* **74**, 011506 (2006).
- <sup>3</sup> C. Reichhardt and C. J. Olson Reichhardt, “Disordering transitions and peak effect in polydisperse particle systems,” *Phys. Rev. E* **77**, 041401 (2008).
- <sup>4</sup> B. Schmittmann and R. K. P. Zia, “Driven diffusive systems. An introduction and recent developments,” *Phys. Rep.* **301**, 45–64 (1998).
- <sup>5</sup> C. J. O. Reichhardt and C. Reichhardt, “Disordering, clustering, and laning transitions in particle systems with dispersion in the Magnus term,” *Phys. Rev. E* **99**, 012606 (2019).
- <sup>6</sup> D. Helbing, I. J. Farkas, and T. Vicsek, “Freezing by heating in a driven mesoscopic system,” *Phys. Rev. Lett.* **84**, 1240–1243 (2000).
- <sup>7</sup> J. Dzubiella, G. P. Hoffmann, and H. Löwen, “Lane formation in colloidal mixtures driven by an external field,” *Phys. Rev. E* **65**, 021402 (2002).
- <sup>8</sup> R. R. Netz, “Conduction and diffusion in two-dimensional electrolytes,” *Europhys. Lett.* **63**, 616–622 (2003).
- <sup>9</sup> M. Ikeda, H. Wada, and H. Hayakawa, “Instabilities and turbulence-like dynamics in an oppositely driven binary particle mixture,” *EPL* **99**, 68005 (2012).
- <sup>10</sup> C. W. Wächter, F. Kogler, and S. H. L. Klapp, “Lane formation in a driven attractive fluid,” *Phys. Rev. E* **94**, 052603 (2016).
- <sup>11</sup> A. Poncet, O. Bénichou, V. Démery, and G. Oshanin, “Universal long ranged correlations in driven binary mixtures,” *Phys. Rev. Lett.* **118**, 118002 (2017).
- <sup>12</sup> N. Bain and D. Bartolo, “Critical mingling and universal correlations in model binary active liquids,” *Nature Commun.* **8**, 15969 (2017).
- <sup>13</sup> C. Reichhardt, J. Thibault, S. Papanikolaou, and C. J. O. Reichhardt, “Laning and clustering transitions in driven binary active matter systems,” *Phys. Rev. E* **98**, 022603 (2018).
- <sup>14</sup> K. A. Bacik, B. S. Bacik, and T. Rogers, “Lane nucleation in complex active flows,” *Science* **379**, 923–928 (2023).
- <sup>15</sup> S. Mühlbauer, B. Binz, F. Jonietz, C. Pfleiderer, A. Rosch, A. Neubauer, R. Georgii, and P. Böni, “Skyrmion lattice in a chiral magnet,” *Science* **323**, 915–919 (2009).
- <sup>16</sup> A. Fert, N. Reyren, and V. Cros, “Magnetic skyrmions: advances in physics and potential applications,” *Nature Rev. Mater.* **2**, 17031 (2017).
- <sup>17</sup> A. Bogdanov and A. Hubert, “Thermodynamically stable magnetic vortex states in magnetic crystals,” *J. Mag. Mag. Mater.* **138**, 255–269 (1994).
- <sup>18</sup> U. K. Röbler, A. N. Bogdanov, and C. Pfleiderer, “Spontaneous skyrmion ground states in magnetic metals,” *Nature (London)* **442**, 797–801 (2006).
- <sup>19</sup> X. Z. Yu, Y. Onose, N. Kanazawa, J. H. Park, J. H. Han, Y. Matsui, N. Nagaosa, and Y. Tokura, “Real-space observation of a two-dimensional skyrmion crystal,” *Nature (London)* **465**, 901–904 (2010).
- <sup>20</sup> T. Schulz, R. Ritz, A. Bauer, M. Halder, M. Wagner, C. Franz, C. Pfleiderer, K. Everschor, M. Garst, and A. Rosch, “Emergent electrodynamics of skyrmions in a chiral magnet,” *Nature Phys.* **8**, 301–304 (2012).
- <sup>21</sup> F. Jonietz, S. Mühlbauer, C. Pfleiderer, A. Neubauer, W. Münzer, A. Bauer, T. Adams, R. Georgii, P. Böni, R. A. Duine, K. Everschor, M. Garst, and A. Rosch, “Spin transfer torques in MnSi at ultralow current densities,” *Science* **330**, 1648–1651 (2010).
- <sup>22</sup> C. Reichhardt and C. J. Olson Reichhardt, “Depinning and nonequilibrium dynamic phases of particle assemblies driven over random and ordered substrates: a review,” *Rep. Prog. Phys.* **80**, 026501 (2017).
- <sup>23</sup> C. Reichhardt, C. J. O. Reichhardt, and M. Milošević, “Statics and dynamics of skyrmions interacting with disorder and nanostructures,” *Rev. Mod. Phys.* **94**, 035005 (2022).
- <sup>24</sup> T. H. R. Skyrme, “A unified field theory of mesons and baryons,” *Nucl. Phys.* **31**, 556 (1962).
- <sup>25</sup> W. Jiang, P. Upadhyaya, W. Zhang, G. Yu, M. B. Jungfleisch, F. Y. Fradin, J. E. Pearson, Y. Tserkovnyak, K. L. Wang, O. Heinonen, S. G. E. te Velthuis, and A. Hoffmann, “Blowing magnetic skyrmion bubbles,” *Science* **349**, 283–286 (2015).
- <sup>26</sup> A. Tonomura, X. Yu, K. Yanagisawa, T. Matsuda, Y. Onose, N. Kanazawa, H. S. Park, and Y. Tokura, “Real-space observation of skyrmion lattice in helimagnet MnSi thin samples,” *Nano Lett.* **12**, 1673–1677 (2012).
- <sup>27</sup> K. Everschor-Sitte and M. Sitte, “Real-space Berry phases: Skyrmion soccer (invited),” *J. Appl. Phys.* **115**, 172602 (2014).
- <sup>28</sup> W. Jiang, X. Zhang, G. Yu, W. Zhang, X. Wang, M. B. Jungfleisch, J. E. Pearson, X. Cheng, O. Heinonen, K. L. Wang, Y. Zhou, A. Hoffmann, and S. G. E. te Velthuis, “Direct observation of the skyrmion Hall effect,” *Nature Phys.* **13**, 162–169 (2017).
- <sup>29</sup> J. Iwasaki, M. Mochizuki, and N. Nagaosa, “Universal current-velocity relation of skyrmion motion in chiral magnets,” *Nature Commun.* **4**, 1463 (2013).
- <sup>30</sup> K. Litzius, I. Lemesh, B. Krüger, P. Bassirian, L. Caretta, K. Richter, F. Büttner, K. Sato, O. A. Tretiakov, J. Förster, R. M. Reeve, M. Weigand, I. Bykova, H. Stoll, G. Schütz, G. S. D. Beach, and M. Kläui, “Skyrmion Hall effect revealed by direct time-resolved X-ray microscopy,” *Nature Phys.* **13**, 170–175 (2017).
- <sup>31</sup> B. Göbel, I. Mertig, and O. A. Tretiakov, “Beyond skyrmions: Review and perspectives of alternative magnetic quasiparticles,” *Phys. Rep.* **895**, 1 (2021).
- <sup>32</sup> A. Bogdanov and A. Hubert, “The stability of vortex-like structures in uniaxial ferromagnets,” *J. Mag. Mag. Mater.* **195**, 182–192 (1999).
- <sup>33</sup> R. Streubel, L. Han, M.-Y. Im, F. Kronast, U. K. Röbler, F. Radu, R. Abrudan, G. Lin, O. G. Schmidt, P. Fischer, and D. Makarov, “Manipulating topological states by imprinting non-collinear spin textures,” *Sci. Rep.* **5**, 8787 (2015).
- <sup>34</sup> J. Hagemester, A. Siemens, L. Rózsa, E. Y. Vedmedenko, and R. Wiesendanger, “Controlled creation and stability of  $k\pi$  skyrmions on a discrete lattice,” *Phys. Rev. B* **97**, 174436 (2018).
- <sup>35</sup> F. Zheng, H. Li, S. Wang, D. Song, C. Jin, W. Wei, A. Kovács, J. Zang, M. Tian, Y. Zhang, H. Du, and R. E. Dunin-Borkowski, “Direct imaging of a zero-field target

- skyrmion and its polarity switch in a chiral magnetic nanodisk,” *Phys. Rev. Lett.* **119**, 197205 (2017).
- <sup>36</sup> A. G. Kolesnikov, M. E. Steblyi, A. S. Samardak, and A. V. Ognev, “Skyrmionium - high velocity without the skyrmion Hall effect,” *Sci. Rep.* **8**, 16966 (2018).
- <sup>37</sup> M. Finazzi, M. Savoini, A. R. Khorsand, A. Tsukamoto, A. Itoh, L. Duò, A. Kirilyuk, Th. Rasing, and M. Ezawa, “Laser-induced magnetic nanostructures with tunable topological properties,” *Phys. Rev. Lett.* **110**, 177205 (2013).
- <sup>38</sup> H. Fujita and M. Sato, “Ultrafast generation of skyrmionic defects with vortex beams: Printing laser profiles on magnets,” *Phys. Rev. B* **95**, 054421 (2017).
- <sup>39</sup> Y. Ishida and K. Kondo, “Theoretical comparison between skyrmion and skyrmionium motions for spintronics applications,” *Japan. J. Appl. Phys.* **59**, SGGI04 (2020).
- <sup>40</sup> J. C. Bellizotti Souza, N. P. Vizarrim, C. J. O. Reichhardt, C. Reichhardt, and P. A. Venegas, “Skyrmionium Dynamics and Stability on One Dimensional Anisotropy Patterns,” (2025).
- <sup>41</sup> X. Zhang, J. Xia, Y. Zhou, D. Wang, X. Liu, W. Zhao, and M. Ezawa, “Control and manipulation of a magnetic skyrmionium in nanostructures,” *Phys. Rev. B* **94**, 094420 (2016).
- <sup>42</sup> Stavros Komineas and Nikos Papanicolaou, “Skyrmion dynamics in chiral ferromagnets under spin-transfer torque,” *Physical Review B* **92**, 174405 (2015).
- <sup>43</sup> S. Komineas and N. Papanicolaou, “Skyrmion dynamics in chiral ferromagnets,” *Phys. Rev. B* **92**, 064412 (2015).
- <sup>44</sup> S. Li, J. Xia, X. Zhang, M. Ezawa, W. Kang, X. Liu, Y. Zhou, and W. Zhao, “Dynamics of a magnetic skyrmionium driven by spin waves,” *Appl. Phys. Lett.* **112**, 142404 (2018).
- <sup>45</sup> J. Xia, X. Zhang, M. Ezawa, O. A. Tretiakov, Z. Hou, W. Wang, G. Zhao, X. Liu, H. T. Diep, and Y. Zhou, “Current-driven skyrmionium in a frustrated magnetic system,” *Appl. Phys. Lett.* **117**, 012403 (2020).
- <sup>46</sup> J. C. Bellizotti Souza, N. P. Vizarrim, C. J. O. Reichhardt, C. Reichhardt, and P. A. Venegas, “Comparing Dynamics, Pinning and Ratchet Effects for Skyrmionium, Skyrmions, and Antiskyrmions,” (2024).
- <sup>47</sup> F. Zheng, N. S. Kiselev, L. Yang, V. M. Kuchkin, F. N. Rybakov, S. Blügel, and R. E. Dunin-Borkowski, “Skyrmion-antiskyrmion pair creation and annihilation in a cubic chiral magnet,” *Nature Phys.* **18**, 863–868 (2022).
- <sup>48</sup> S. Wang, L. Qiu, and K. Shen, “Nonvolatile current-induced topological charge imbalance of magnetic textures,” *Commun. Phys.* **8**, 43 (2025).
- <sup>49</sup> Y. Zhang, J. Tang, Y. Wu, M. Shi, X. Xu, S. Wang, M. Tian, and H. Du, “Stable skyrmion bundles at room temperature and zero magnetic field in a chiral magnet,” *Nature Commun.* **15**, 3391 (2024).
- <sup>50</sup> F. Zheng, F. N. Rybakov, A. B. Borisov, D. Song, S. Wang, Z.-A. Li, H. Du, N. S. Kiselev, J. Caron, A. Kovacs, M. Tian, Y. Zhang, S. Blügel, and R. E. Dunin-Borkowski, “Experimental observation of chiral magnetic bobsers in B20-type FeGe,” *Nature Nanotechnol.* **13**, 451–455 (2018).
- <sup>51</sup> A.-O. Mandru, O. Yildirim, R. Tomasello, P. Heistracher, M. Penedo, A. Giordano, D. Suess, G. Finocchio, and H. J. Hug, “Coexistence of distinct skyrmion phases observed in hybrid ferromagnetic/ferrimagnetic multilayers,” *Nature Commun.* **11**, 6365 (2020).
- <sup>52</sup> H. R. O. Sohn, C. D. Liu, and I. I. Smalyukh, “Schools of skyrmions with electrically tunable elastic interactions,” *Nature Commun.* **10**, 4744 (2019).
- <sup>53</sup> R. C. V. Coelho, H. Zhao, M. Tasinkevych, I. I. Smalyukh, and M. M. Telo da Gama, “Sculpting liquid crystal skyrmions with external flows,” *Phys. Rev. Res.* **5**, 033210 (2023).
- <sup>54</sup> G. N. C. Amaral, H. Zhao, M. Sedahmed, T. Campante, I. I. Smalyukh, M. Tasinkevych, M. M. Telo da Gama, and R. C. V. Coelho, “Liquid crystal torons in Poiseuille-like flows,” *Sci. Rep.* **15**, 2684 (2015).
- <sup>55</sup> Richard F L Evans, “Atomistic Spin Dynamics,” in *Handbook of Materials Modeling: Applications: Current and Emerging Materials*, edited by Wanda Andreoni and Sidney Yip (Springer International Publishing, 2018) pp. 1–23.
- <sup>56</sup> Junichi Iwasaki, Masahito Mochizuki, and Naoto Nagaosa, “Current-induced skyrmion dynamics in constricted geometries,” *Nature Nanotechnology* **8**, 742–747 (2013).
- <sup>57</sup> S. Paul, S. Haldar, S. von Malottki, and S. Heinze, “Role of higher-order exchange interactions for skyrmion stability,” *Nature Commun.* **11**, 4756 (2020).
- <sup>58</sup> Shinichiro Seki and Masahito Mochizuki, *Skyrmions in Magnetic Materials* (Springer International Publishing, 2016) series Title: SpringerBriefs in Physics.
- <sup>59</sup> T. L. Gilbert, “A phenomenological theory of damping in ferromagnetic materials,” *IEEE Trans. Mag.* **40**, 3443–3449 (2004).
- <sup>60</sup> O. Boule, J. Vogel, H. Yang, S. Pizzini, D. de Souza Chaves, A. Locatelli, T. O. Mentes, A. Sala, L. D. Buda-Prejbeanu, O. Klein, M. Belmeguenai, Y. Roussigné, A. Stashkevich, S. M. Chérif, L. Aballe, M. Foerster, M. Chshiev, S. Auffret, I. M. Miron, and G. Gaudin, “Room-temperature chiral magnetic skyrmions in ultrathin magnetic nanostructures,” *Nature Nanotechnol.* **11**, 449–454 (2016).
- <sup>61</sup> J. Kiefer and J. Wolfowitz, “Stochastic estimation of the maximum of a regression function,” *Annal. Math. Stat.* **23**, 462–466 (1952).
- <sup>62</sup> H. Robbins and S. Monro, “A stochastic approximation method,” *Annal. Math. Stat.* **22**, 400–407 (1951).
- <sup>63</sup> S.-Z. Lin, C. Reichhardt, C. D. Batista, and A. Saxena, “Particle model for skyrmions in metallic chiral magnets: Dynamics, pinning, and creep,” *Phys. Rev. B* **87**, 214419 (2013).
- <sup>64</sup> E. Raimondo, E. Saugar, J. Barker, D. Rodrigues, A. Giordano, M. Carpentieri, W. Jiang, O. Chubykalo-Fesenko, R. Tomasello, and G. Finocchio, “Temperature-gradient-driven magnetic skyrmion motion,” *Phys. Rev. Appl.* **18**, 024062 (2022).
- <sup>65</sup> S. L. Zhang, W. W. Wang, D. M. Burn, H. Peng, H. Berger, A. Bauer, C. Pfeleiderer, G. van der Laan, and T. Hesjedal, “Manipulation of skyrmion motion by magnetic field gradients,” *Nature Commun.* **9**, 2115 (2018).
- <sup>66</sup> A. Jiang, Y. Zhou, X. Zhang, and M. Mochizuki, “Transformation of a skyrmionium to a skyrmion through the thermal annihilation of the inner skyrmion,” *Phys. Rev. Res.* **6**, 013229 (2024).